The Shape, Propagation and Mean-Flow Interaction of Large-Scale Weather Systems

BRIAN J. HOSKINS, IAN N. JAMES AND GLENN H. WHITE[1]

Department of Meteorology, University of Reading, Reading, U.K.

(Manuscript received 1 November 1982, in final form 18 February 1983)

ABSTRACT

For a zonal averaging operator the Eliassen–Palm flux provides a diagnostic of both eddy behavior and the feedback of the eddies onto the mean flow. This paper addresses the diagnosis problem for other averaging operators and, in particular, for time averaging which has proved in recent years such a powerful means of viewing the three-dimensional tropospheric flow. The horizontal velocity correlation tensor gives a measure of the characteristic horizontal eddy shape at a point. It also implies the direction of the group velocity relative to the mean flow in cases where such a concept is valid. However the major emphasis here is on the mean-flow feedback of eddies. In this respect, the eddy vorticity flux is determined by derivatives of the components of the anisotropic part of the tensor. Making a reasonable approximation allows the eddy vorticity flux convergence to be written in terms of $\mathbf{E} = (\overline{v'^2} - \overline{u'^2}, -\overline{u'v'})$. A simple interpretation of the mean flow feedback of eddies is then possible. A slightly more restrictive approximation allows the eddy shape and the sense of the relative group velocity to be determined also from $\mathbf{E}$. The whole analysis may also be performed in the three-dimensional quasi-geostrophic case where it provides an approximate extension of the Eliassen–Palm flux concept.

The theory and approximations are investigated for high-pass and low-pass transient eddies using data for single Northern and Southern Hemisphere winter seasons. The different signatures of the transient eddies in the two frequency bands are apparent and schematic pictures of the contrasting, dominant behavior in each band emerge. Data from one particular blocking event, when diagnosed using the theory developed here, give an indication of a positive feedback of the synoptic eddies onto the mean blocking flow.

1. Introduction

One of the ever present problems in understanding the general circulation of the atmosphere is the determination of the role of the large-scale eddies and of ways of understanding their behavior and their feedback onto the mean flow. For many years the poleward heat flux by eddies has been considered important. Since the work of Jeffreys (1926) the importance of the eddy poleward westerly momentum flux in zonally averaged budgets has also been emphasized. However, the more recent studies of Blackmon *et al.* (1977) and others suggest that using a time-averaging operator yields a mean flow in which the role of the eddies, i.e. the transients, may be rather different. Neglecting vertical advection and approximating the Coriolis parameter by a constant value f_0, the time-mean zonal momentum equation may be written

$$\bar{u}\bar{u}_x + \bar{v}\bar{u}_y = f_0\bar{v}_a - (\overline{u'^2})_x - (\overline{u'v'})_y,$$

where the bar signifies a time average and the prime a deviation from this average. In both jet entrance and exit regions the dominant balance is $\bar{u}\bar{u}_x \sim f_0\bar{v}_a$, there being poleward ageostrophic motion in the entrance and equatorward motion in the exit. The eddy flux convergence terms are small. However, as discussed in Hoskins (1983), in the meridional momentum equation the eddy flux convergence $-(\overline{v'^2})_y$ appears to be significantly larger than the mean flow advection and must be balanced by $f_0\bar{u}_a$. Here, $\bar{u}_a$ could be the x-component of a mean horizontally non-divergent circulation: $= f_0^{-1}[-(\overline{v'^2})_y, (\overline{v'^2})_x]$. The y-component of this circulation would give a term $(\overline{v'^2})_x$ as a forcing term on the rhs of the zonal momentum equation which, though larger than the other eddy terms, is probably still small compared with the mean acceleration. This argument is heuristic, and it is clearly necessary to consider the role of eddies in the mean vorticity and potential vorticity equations as has been done by Savijarvi (1977, 1978), Holopainen (1978), Lau (1979), Holopainen and Oort (1981), and Holopainen *et al.* (1982). One difficulty with such studies is that transient eddy vorticity flux convergences are very noisy quantities due to the high number of derivatives involved and that simple arguments as to what features of the eddies imply these convergences are not available.

For the zonally-averaged problem a recent diagnostic that has proved very valuable is the Eliassen–Palm (EP) flux of Andrews and McIntyre (1976), discussed also in Edmon *et al.* (1980). It has minus the poleward westerly momentum flux as its y component, while its vertical component is proportional

[1] Present affiliation: Goddard Laboratory for Atmospheric Sciences, NASA/Goddard Space Flight Center, Code 911, Greenbelt, MD 20771.

to the poleward heat flux. The EP flux gives information on the meridional-vertical propagation of waves, occurs as a flux in an eddy conservation relation, and describes the feedback of the eddies onto the zonally averaged flow. The aim of this paper is to present a theory which, in some ways, provides an extension of the Eliassen–Palm flux concept so that it can be applied in particular to the time-averaged three space dimension problem. The emphasis is on the understanding of the feedback of the eddies onto the mean flow, but the behavior of the eddies themselves is also discussed.

Section 2 considers the horizontal velocity correlation tensor and shows how this gives information on characteristic eddy shape and barotropic group velocity. Under certain restrictive conditions the eddy conservation relation of Young and Rhines (1980) is obtained. The mechanical feedback of the eddies onto the mean flow is shown to be given by derivatives of the anisotropic part of the velocity correlation tensor, the isotropic part appearing only in the mean balance equation. The understanding of this feedback is greatly simplified by an approximation which is introduced in Section 3. The mechanical effect of the eddies is then summarized by the quantity $\mathbf{E} = (\overline{v'^2} - \overline{u'^2}, -\overline{u'v'})$. In most cases, the information on eddy shape and group velocity is also contained in $\mathbf{E}$. In Section 4 the theory is extended to a baroclinic quasi-geostrophic atmosphere. The approximations made and the diagnostics suggested in Sections 2–4 are illustrated by calculations for the Northern Hemisphere 1979–80 winter, using analyzed data from the European Centre for Medium Range Weather Forecasts. The mean 250 mb streamfunction contours and major jets for this winter are shown in Fig. 1. As usual for the winter season, the westerly flow strengthens over North Africa and remains rather constant across Asia before achieving a strong maximum of 65 m s^{-1} just off the east coast of Asia. Centered on the east coast of North America is a 45 m s^{-1} westerly jet of rather more limited zonal extent. Statistics are presented below for high- and low-pass transient eddies with periods shorter and longer than 10 days, respectively. Details of the data source and manipulation are given in Appendix B.

In Section 5 some diagnostics for the Southern Hemisphere are presented. Section 6 includes schematic pictures of winter high-pass and low-pass transients and also an indication of transient behavior in one particular blocking regime. Appendix A contains an alternative derivation of the importance of $\mathbf{E}$ in the mean flow forcing based on the momentum equations.

2. Basic barotropic theory

It is convenient to begin the discussion by considering the horizontal velocity correlation tensor $\overline{v_i'v_j'}$

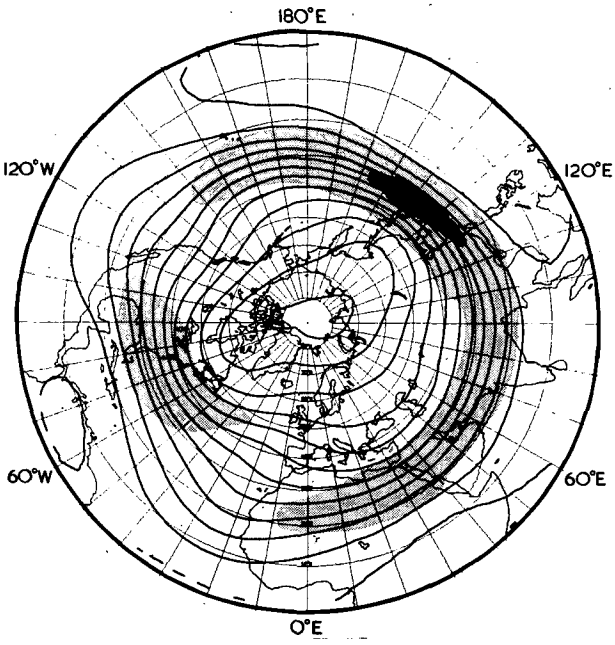

FIG. 1. The mean streamfunction $\bar{\psi}$ at 250 mb for the period 1 December 1979–29 February 1980, Northern Hemisphere. Contour interval is 12.7×10^6 m^2 s^{-1} (thus, one contour interval spread over 10° of latitude corresponds to a wind speed of 11.5 m s^{-1}); this and subsequent similar plots are all given on a polar stereographic map projection. Light shading indicates wind speeds in excess of 30 m s^{-1} and heavy shading wind speeds greater than 60 m s^{-1}. The characteristic jets over North America, North Africa and east Asia are all well represented.

where the bar signifies an averaging operator and the prime a deviation from this average. This symmetric tensor is easily separated into its isotropic and anisotropic (trace-free) parts:

$$\mathbf{C} \equiv \begin{pmatrix} \overline{u'^2} & \overline{u'v'} \\ \overline{u'v'} & \overline{v'^2} \end{pmatrix} = \begin{pmatrix} K & 0 \\ 0 & K \end{pmatrix} + \mathbf{A}, \tag{1}$$

where

$$\mathbf{A} = \begin{pmatrix} M & N \\ N & -M \end{pmatrix}, \tag{2}$$

and

$$K = \tfrac{1}{2}(\overline{u'^2 + v'^2}), \quad M = \tfrac{1}{2}(\overline{u'^2 - v'^2}),$$
$$N = \overline{u'v'}. \tag{3}$$

Here, K is the kinetic energy of the eddies. Relative to tilde axes rotated by an angle θ from the basic zonal and meridional axes,

$$\mathbf{A} = \begin{pmatrix} \tilde{M} & \tilde{N} \\ \tilde{N} & -\tilde{M} \end{pmatrix}, \tag{4}$$

where

$$(\tilde{M}, \tilde{N}) = (M\cos 2\theta + N \sin 2\theta,$$
$$-M \sin 2\theta + N \cos 2\theta). \tag{5}$$

For example, for axes rotated by 45° from the basic axes,

$$\tilde{M} = \tfrac{1}{2}(\overline{\tilde{u}'^2 - \tilde{v}'^2}) = N = \overline{u'v'}. \quad (6)$$

From (5), the principal axes of **A** or **C** are at angles $\frac{1}{2}\tan^{-1}(N/M)$ with the x axis. Taking the $\hat{x}$ axis to be along the major axis, at an angle

$$\theta = \tfrac{1}{2}\sin^{-1}[N/(M^2 + N^2)^{1/2}], \quad (7)$$

we have

$$(\hat{M}, \hat{N}) = [(M^2 + N^2)^{1/2}, 0]. \quad (8)$$

Since $\hat{M} = \frac{1}{2}(\overline{\hat{u}'^2 - \hat{v}'^2})$ and $K = \frac{1}{2}(\overline{\hat{u}'^2 + \hat{v}'^2})$, we must have $\hat{M} \leq K$, with equality only if $\hat{v}'^2 = 0$. If the eddies are approximately horizontally non-divergent and locally have a streamfunction of the form

$$\psi = \hat{\psi}\cos k(\hat{x} - c_1 t)\cos l(\hat{y} - c_2 t), \quad (9)$$

then

$$\hat{M} \propto l^2 - k^2,$$

provided that the averaging operator averages over the phases of the streamfunction. For c_1 and c_2 nonzero, the result is valid in particular for a simple time average of sufficient length. Thus, eddies are locally extended along the major axis and compressed along the minor axis. The quantity $\alpha = \hat{M}K$ which lies between 0 and 1 provides a dimensionless measure of eddy anisotropy. For the simple case discussed above, $\alpha = (l^2 - k^2)/(l^2 + k^2)$.

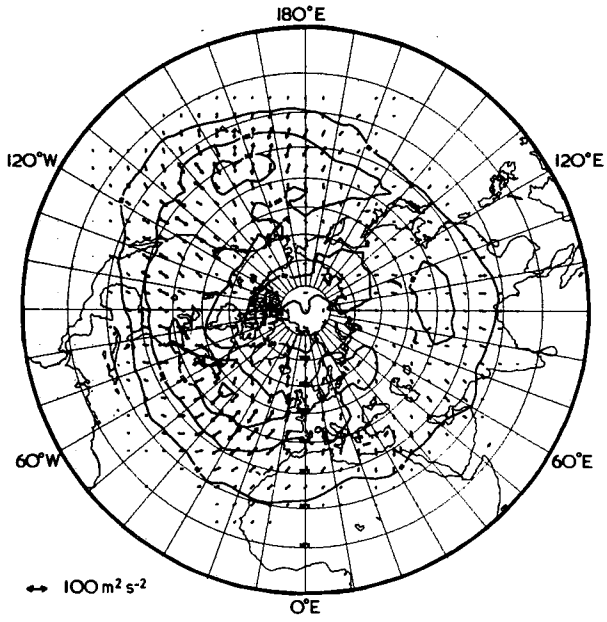

FIG. 2. An illustration of the velocity correlation tensor for the high-pass filtered eddies (i.e., with periods shorter than 10 days) at 250 mb during the 1979–80 Northern Hemisphere winter. Contours show $K = \frac{1}{2}(u'^2 + v'^2)$ (interval 50 m² s⁻²), while the vectors are of length $\hat{M}$ and in the direction of the major axis of **A**. The major axes of the eddies are generally oriented north–south. The Atlantic and Pacific storm tracks can be seen in both the K and $\hat{M}$ fields.

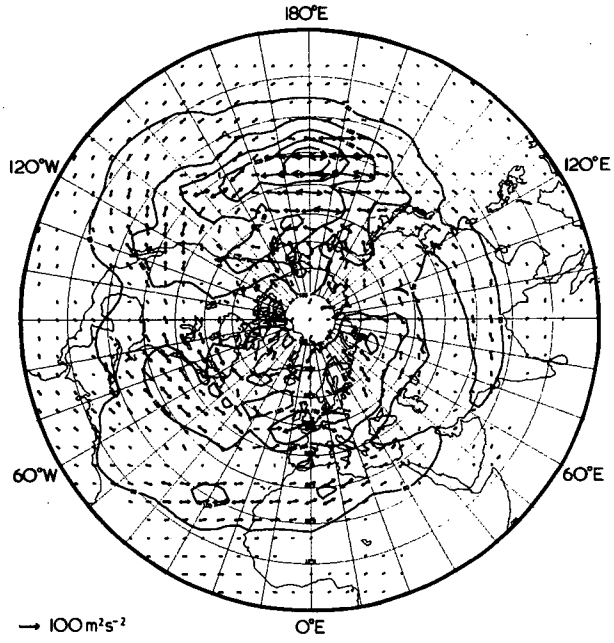

FIG. 3. As in Fig. 2, but for the low-pass filtered eddies (i.e., with periods greater than 10 days). The major axes of **A** and of the eddies are generally aligned east–west. Note the intense maxima of both K and $\hat{M}$ in the mid-Pacific.

The velocity correlation tensor for the high pass eddies in the Northern Hemisphere (1979–80 winter is summarized in Fig. 2. This shows contours of eddy kinetic energy K and lines indicating the direction of the major axes of **A** and of length proportional to $\hat{M}$. It may be noted that the Pacific storm track was unusually weak during this year. Looking at the Atlantic storm track in particular, it is evident that the axes are predominantly north-south indicating that the high-pass eddies are mostly elongated meridionally. Typical values of α are of order 0.4, implying a ratio of meridional to zonal scales of about 3 to 2. They also reflect the "tilted trough" structure of the eddies, showing a SW–NE orientation to the south of and near the end of the storm track and a NW–SE orientation to the north. This picture of the high-pass eddies is consistent with that obtained from grid point correlations of high pass filtered height field data (Blackmon *et al.*, 1983). For reference below, we note that typical storm-track magnitudes of K, M and N are 150, −50 and ±25 m² s⁻², respectively.

An entirely different picture emerges for the low-pass transients (Fig. 3). The major axes are mostly in the east–west direction, indicating that these eddies are predominantly elongated zonally. Again this is consistent with the low-frequency height field signatures found by Wallace and Gutzler (1981) and others. It is evident that there is a dramatic change in transient eddy character near the one-week timescale. Very large values of $\hat{M}$ are found in the exit region of the Pacific jet, where the anisotropy number

α has large values, typically 0.7. This implies a ratio of zonal to meridional scales of the order 5 to 2.

In simple situations, the anisotropic velocity correlation tensor provides information not only on the structure of the eddies but also on the propagation of eddy activity. The WKBJ conditions (see, e.g., Dingle, 1973) of slow mean flow variation and locally sinusoidal waves are assumed and the atmosphere is taken to be barotropic. If $\bar{\zeta}$ is the time-mean absolute vorticity, then the dispersion relation for waves whose local streamfunction is $\psi' = A\cos(kx + ly - \omega t)$ is

$$\omega = k\bar{u} + l\bar{v} - (k\bar{\zeta}_y - l\bar{\zeta}_x)/(k^2 + l^2). \quad (10)$$

Then the x and y components of group velocity are

$$c_1 = \frac{\partial\omega}{\partial k} = \bar{u} + \frac{[(k^2 - l^2)\bar{\zeta}_y - 2kl\bar{\zeta}_x]}{(k^2 + l^2)^2}, \quad (11)$$

$$c_2 = \frac{\partial\omega}{\partial l} = \bar{v} + \frac{[2kl\bar{\zeta}_y + (k^2 - l^2)\bar{\zeta}_x]}{(k^2 + l^2)^2}. \quad (12)$$

If the averaging operator averages the phases of the wave sufficiently,

$$\frac{M}{\frac{1}{2}\overline{\zeta'^2}} = \frac{(l^2 - k^2)}{(k^2 + l^2)^2}, \quad (13)$$

$$\frac{N}{\frac{1}{2}\overline{\zeta'^2}} = -\frac{2kl}{(k^2 + l^2)^2}. \quad (14)$$

Therefore

$$\tfrac{1}{2}\overline{\zeta'^2}(\mathbf{c}_g - \bar{\mathbf{v}}) = (-M\bar{\zeta}_y + N\bar{\zeta}_x, -M\bar{\zeta}_x - N\bar{\zeta}_y). \quad (15)$$

Relative to axes along and across the mean absolute vorticity contours, this implies

$$\tfrac{1}{2}\overline{\zeta'^2}(\mathbf{c}_g - \bar{\mathbf{v}}) = -|\nabla\bar{\zeta}|(\tilde{M}, \tilde{N})$$
$$= -|\nabla\bar{\zeta}|\tilde{M}(\sin 2\gamma), \quad (16)$$

where γ is the angle that the anisotropy axis makes with the absolute vorticity contours and ∇ is the horizontal gradient operator. Examples of possible situations are given in Fig. 4.

The linearised eddy barotropic vorticity equation may be written

$$(\partial_t + \bar{\mathbf{v}}\cdot\nabla)\zeta' + \mathbf{v}'\cdot\nabla\bar{\zeta} = \mathcal{D}', \quad (17)$$

where $\mathcal{D}'$ represents source and sink terms. Multiplication by ζ' and averaging gives the eddy enstrophy equation

$$(\partial_t + \bar{\mathbf{v}}\cdot\nabla)\tfrac{1}{2}\overline{\zeta'^2} = -\overline{\mathbf{v}'\zeta'}\cdot\nabla\bar{\zeta} + \overline{\mathcal{D}'\zeta'}. \quad (18)$$

Using rectangular Cartesian axes, the eddy vorticity is $\zeta' = v'_x - u'_y$. Assuming horizontal non-divergence of the eddies, it is easily shown that the eddy vorticity may be written

$$\overline{\mathbf{v}'\zeta'} = (-M_y + N_x, -M_x - N_y). \quad (19)$$

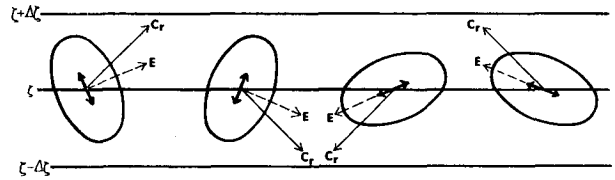

FIG. 4. Illustrating the relative orientations of the eddy anisotropy axis, the E vector (defined below in Section 3) and the group velocity relative to the mean flow $\mathbf{c}_r = \mathbf{c}_g - \bar{\mathbf{v}}$. The left-hand pair show configurations characteristic of the high frequency transients while those on the right are typical of the low frequency transients.

Substituting in (18) yields

$$(\partial_t + \bar{\mathbf{v}}\cdot\nabla)\tfrac{1}{2}\overline{\zeta'^2}$$
$$= (M_y - N_x)\bar{\zeta}_x + (M_x + N_y)\bar{\zeta}_y + \overline{\mathcal{D}'\zeta'}$$
$$= -(-M\bar{\zeta}_y + N\bar{\zeta}_x)_x - (-M\bar{\zeta}_x - N\bar{\zeta}_y)_y + \overline{\mathcal{D}'\zeta'},$$

provided that derivatives in the mean flow vorticity gradients are neglected compared with those of the eddy quantities M and N. This is a very restrictive condition. It is certainly satisfied in cases in which β dominates the vorticity gradient but is probably a poor approximation in most tropospheric applications. From (15), the terms on the rhs may be rewritten in terms of the group velocity and the enstrophy equation takes the conservation form:

$$(\tfrac{1}{2}\overline{\zeta'^2})_t + \nabla\cdot(\mathbf{c}_g\tfrac{1}{2}\overline{\zeta'^2}) = \overline{\mathcal{D}'\zeta'}. \quad (20)$$

This equation has been derived more elegantly by Young and Rhines (1980). In the absence of dissipation and transience, enstrophy density is conserved following the group velocity.

We now turn from the structure and propagation of eddies to their feedback onto the mean flow. This problem was the origin of the present study and remains its dominant theme. At the level of quasi-geostrophic theory, the equation for the mean absolute vorticity $\bar{\zeta}$ may be written

$$(\partial_t + \bar{\mathbf{v}}\cdot\nabla)\bar{\zeta} + f\bar{D} + \nabla\cdot\overline{\mathbf{v}'\zeta'} = \mathbf{k}\cdot\nabla\times\bar{\mathbf{F}}, \quad (21)$$

where D is the divergence and $\mathbf{F}$ the frictional force which will be assumed for convenience to be negligible except in the boundary layer. Denoting a vertical p-integral by [ ] and taking $[D] \approx 0$, the vertical integral of (21) gives

$$[(\partial_t + \bar{\mathbf{v}}\cdot\nabla)\bar{\zeta}] + [\nabla\cdot\overline{\mathbf{v}'\zeta'}] = -g\mathbf{k}\cdot\nabla\times\boldsymbol{\tau}_s, \quad (22)$$

where $\boldsymbol{\tau}_s$ is the surface stress. The eddies contribute to the vertically averaged, mean vorticity budget through the eddy vorticity flux divergence and, possibly, through their modification of the mean surface

stress. As pointed out by Holopainen (1978) and is clear from (19) this divergence at any level may be written

$$\nabla \cdot \overline{\mathbf{v}'\zeta'} = -2M_{xy} + N_{xx} - N_{yy}. \quad (23)$$

Thus the barotropic part of eddy forcing of the mean flow is also determined by the eddy anisotropy.

A direct evaluation of (23) yields a field whose large-scale structure is obscured by small-scale noise. This problem is overcome by computing

$$S = -\nabla^{-2}(\nabla \cdot \overline{\mathbf{v}'\zeta'}), \quad (24)$$

which, from (21), may be considered to be the forcing of the mean streamfunction. This diagnostic, vertically averaged from 700 to 300 mb, was also computed by Holopainen *et al.* (1982) from 8 winters of twice daily analyses produced by the U.S. National Meteorological Center. Since the vertical integral of S is dominated by contributions from levels near the tropopause, Fig. 5 shows the contours of S just at 250 mb for the Northern Hemisphere 1979–80 winter high-pass (Fig. 5a) and low-pass (Fig. 5c) eddies. The most pronounced feature in Fig. 5a is the anticyclonic forcing to the south of the Atlantic storm track, leading to a generally westerly acceleration, of the order of 5 m s^{-1} day^{-1}, along the storm track. There is a similar, although much weaker, feature in the Pacific. Qualitatively, it resembles the forcing found by Holopainen *et al.* (1982; see their Fig. 6) except that there the acceleration in the Pacific storm track was stronger. The higher level of the present data, and the unusually weak Pacific storm track in the 1979–80 winter are sufficient to account for these differences.

Fig. (5c) shows a much more intense forcing by the low frequency transients, with an especially noteworthy "quadrupole" structure of forcing in the mid-Pacific. A weaker quadrupole can be discerned in the western Atlantic. A comparison with the corresponding field in Holopainen *et al.* (1982; their Fig. 6) shows good qualitative agreement north of 40°N. However, south of this latitude the fields are much flatter than in Fig. 5c and the quadrupole structure in the Pacific is not revealed. These differences probably illustrate the large effect that the spurious boundary at 20°N in the NMC analyses can have on such a diagnostic.

Having shown the importance of the anisotropic part of the eddy velocity correlation tensor in forcing the mean flow, it is worth noting the role of the isotropic, kinetic energy portion. It may be shown, as in Hoskins (1983), that the divergence of the approximated horizontal momentum equation yields the "balance equation" for the mean ageostrophic vorticity. Using standard notation, this may be written

$$f_0\bar{\zeta}_a = 2(\bar{\psi}_{xy}^2 - \bar{\psi}_{xx}\bar{\psi}_{yy}) + \beta\bar{\psi}_y - \mathbf{k} \cdot \nabla \times \overline{\mathbf{v}'\zeta'} + \nabla^2 K. \quad (25)$$

As discussed by Hoskins, the kinetic energy term dominates the high-pass transient eddy contribution so that a storm track maximum of K tends to be associated with negative mean ageostrophic vorticity. This would be of importance only if one wished to obtain a mean height field from the mean vorticity.

3. An approximation

The discussion in Section 2 showed that M and N give the feedback of the eddies onto the mean flow as well as an indication of eddy structure and propagation. However, there is a limit to the usefulness of the theory in giving qualitative understanding of flow situations. This is because of the difficulty in dealing with the axis and magnitude of a second order tensor, because of the second derivatives occurring in the eddy vorticity flux divergence and also because of the inherent noisiness of this latter quantity. However, a great simplification is possible if an approximation is made.

In the mean vorticity equation, the mechanical effect of the eddies is represented by the eddy vorticity flux divergence which may be written in terms of M and N as in (23). The term N_{xx} may be neglected if at least one of the following is true:

1) The x-length scale of N is much larger than its y-length scale.
2) The M term in (23) dominates the N terms.

For the high-pass eddies in their elongated storm tracks, condition 1) is usually well-satisfied. In most regions, during most periods condition 2) is satisfied for the low-pass eddies. As a partial check on the validity of neglecting the term N_{xx}, the mean streamfunction forcing S defined by (24) and (23) has been recomputed for the same case as before but with this term omitted. The high-pass eddy picture in Fig. 5b should be compared with the full form in Fig. 5a. The features in the approximated version are generally very well represented, though the amplitude of some features is slightly reduced. The agreement between the approximated (Fig. 5d) and full (Fig. 5c) forms for the low-pass eddies is less exact, although the qualitative form of the fields is quite acceptable in the approximated version. It is scarcely surprising that a number of small-scale features at high latitudes are not captured.

The mean-flow forcing by high-pass eddies and in most places by the low-pass eddies is therefore well approximated by

$$\nabla \cdot \overline{\mathbf{v}'\zeta'} = -2M_{xy} - N_{yy} = \partial_y \nabla \cdot \mathbf{E}, \quad (26)$$

where the quasi-vector[2]

$$\mathbf{E} = (-2M, -N) = (\overline{v'^2 - u'^2}, -\overline{u'v'}). \quad (27)$$

[2] As will be discussed below, E does not transform as a true vector.

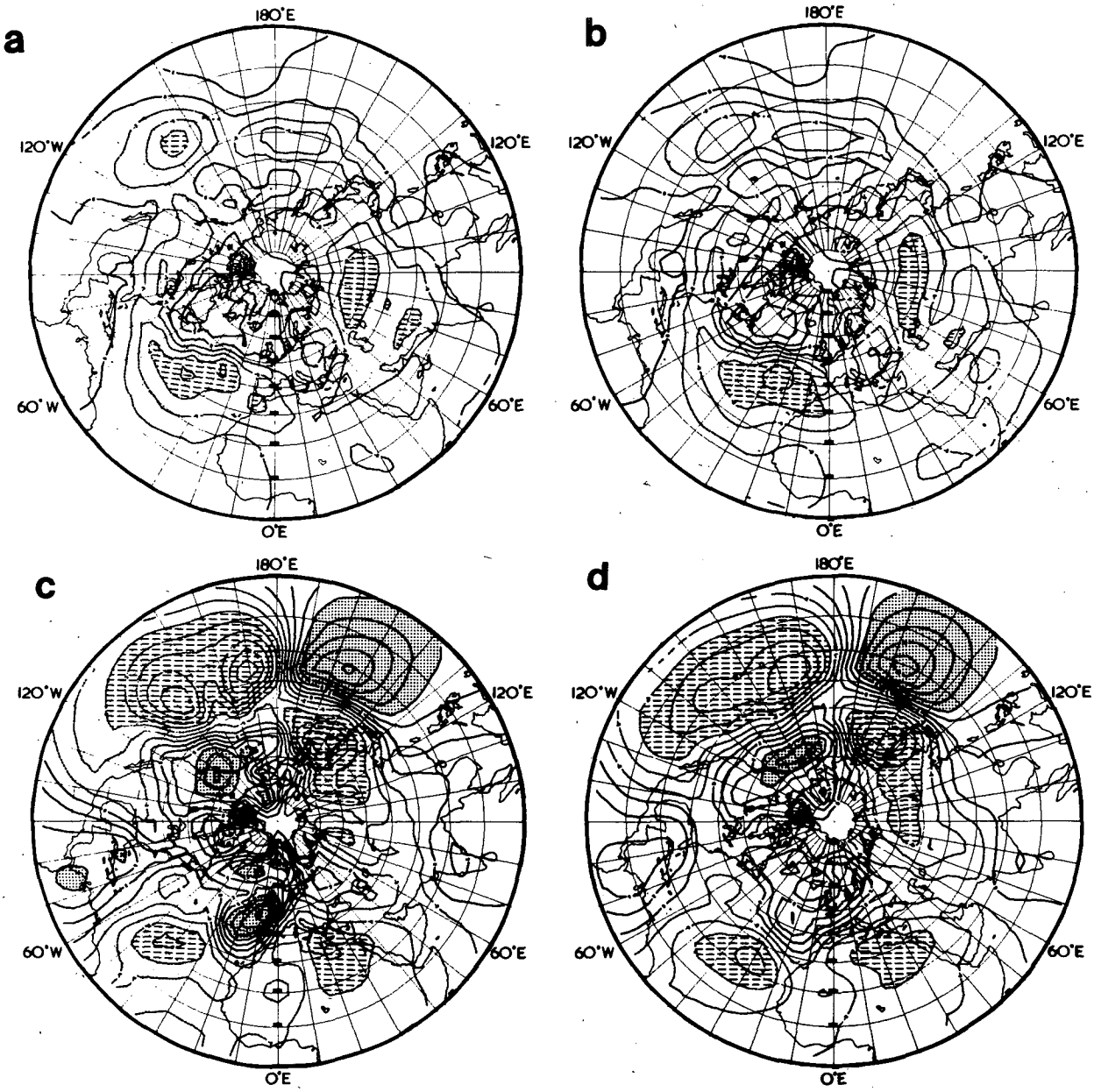

FIG. 5. $S = -\nabla^{-2}(\nabla \cdot \overline{\mathbf{v}'\zeta'})$ for the 1979–80 Northern Hemisphere winter at 250 mb. The contour interval is 12.7 $m^2\ s^{-2}$ (so that one contour interval spread over 10° of latitude corresponds to an acceleration of 1 $m\ s^{-1}\ day^{-1}$), and negative contours are shown by pecked contours. The dashes indicate values less than $-76.2\ m^2\ s^{-2}$ and the stipples values in excess of $+76.2\ m^2\ s^{-2}$. (a) Exact form, with $\nabla \cdot \overline{\mathbf{v}'\zeta'} = -2M_{xy} + N_{xx} - N_{yy}$, high-pass transients. (b) Approximate form, $\nabla \cdot \overline{\mathbf{v}'\zeta'} \approx -2M_{xy} - N_{yy} = \partial_y \nabla \cdot \mathbf{E}$, high pass transients. (c) Exact form, low-pass transients. (d) Approximate form, low-pass transients. The approximation is good for the high-pass eddies and, apart from small scale features at high latitudes, satisfactory for the low-pass eddies.

Since the mean vorticity is $\bar{\zeta} = f + \bar{v}_x - \bar{u}_y$, the eddy vorticity flux divergence occurs in the mean vorticity equation (21) as if there were an eddy x-momentum flux

$$-\mathbf{E} = (\overline{u'^2 - v'^2}, \overline{u'v'}). \tag{28}$$

The occurrence of $\overline{v'^2}$ in this expression is entirely consistent with the heuristic arguments in the introduction. $-\mathbf{E}$ may be considered as an effective westerly momentum flux, though its rigorous interpretation is in terms of the forcing of mean horizontal circulation. Where $\mathbf{E}$ is divergent there is a forcing of mean horizontal circulation consistent with a tendency to increase westerly mean flow. Where $\mathbf{E}$ is convergent, the mean flow circulation forcing is consistent with a tendency to decrease westerly mean

flow. A direct demonstration of the importance of $\nabla \cdot \mathbf{E}$ in the x-momentum equation is given in Appendix A.

Plots of $\mathbf{E}$ for the high-pass and low-pass transient eddies during the Northern Hemisphere 1979–80 winter are given in Fig. 6. The high-pass eddies in the Atlantic storm track show a divergence of $\mathbf{E}$ from the start and middle of the storm track which is consistent with the mean westerly forcing there, and a tendency by the eddies to extend the strong westerly flow further across the Atlantic. A similar, but weaker, pattern is associated with the Pacific storm track. The low-pass eddies in the Pacific jet exit give a strong convergence of $\mathbf{E}$ in mid-latitudes near 160°E and strong divergence further downstream. The corresponding intense easterly mean flow forcing near 160°E, where the west wind is strong, and westerly mean flow forcing downstream, where the west wind is weaker, can be seen in Fig. 5c.

A slightly more restrictive approximation allows the eddy structure and propagation characteristics implicit in the tensor $\mathbf{A}$ to be determined also from $\mathbf{E}$. It was evident from Figs. 2 and 3 that the principal axes of $\mathbf{A}$ are mostly inclined at only small angles with the zonal and meridional directions ($|M| \gg |N|$). This was particularly true for the high-pass eddies. For the axis making only a small angle with the zonal direction its angle is

$$\tfrac{1}{2} \tan^{-1}(N/M) \approx \tan^{-1}(N/2M).$$

The error involved is only 5% for $M = 2N$. Then, to order N^2/M^2, $\mathbf{E}$ is parallel to the axis making a small angle with the zonal direction, and its magnitude is $2\hat{M}$. For the various eddy orientations shown above in the schematic Fig. 4, the relevant directions for $\mathbf{E}$ are also indicated. For meridionally elongated eddies, $\mathbf{E}$ points eastwards along the minor axis, whilst for zonally elongated eddies it points westwards along the major axis. Provided that the mean absolute vorticity contours make only small angles with the zonal direction, the relationship between $\mathbf{E}$ and the group velocity as described by (16) is the simple one shown in Fig. 4. The relative group velocity $\mathbf{c}_g - \bar{\mathbf{v}}$ subtends an angle with $\mathbf{E}$ equal to that made by the mean vorticity contour.

Comparison of Fig. 6a and Fig. 2 indicates that, for the high-pass eddies, almost everywhere the magnitude $\hat{M}$ and the direction of the minor axis are well represented by $\mathbf{E}$. The arrows reflect the predominance of meridionally elongated eddies. The fanning out of the arrows along the storm track is associated with the tilting of troughs. In barotropic group velocity terms, wave activity propagates downstream faster than the flow and towards the end of the track the propagation has a significant equatorward component. For the low-pass eddies, comparison of Fig. 6b with Fig. 3 shows that the direction of the major axis and the magnitude $\hat{M}$ are generally given well by $\mathbf{E}$. Particularly near the date line Fig. 6b indicates the predominance of zonally elongated eddies with

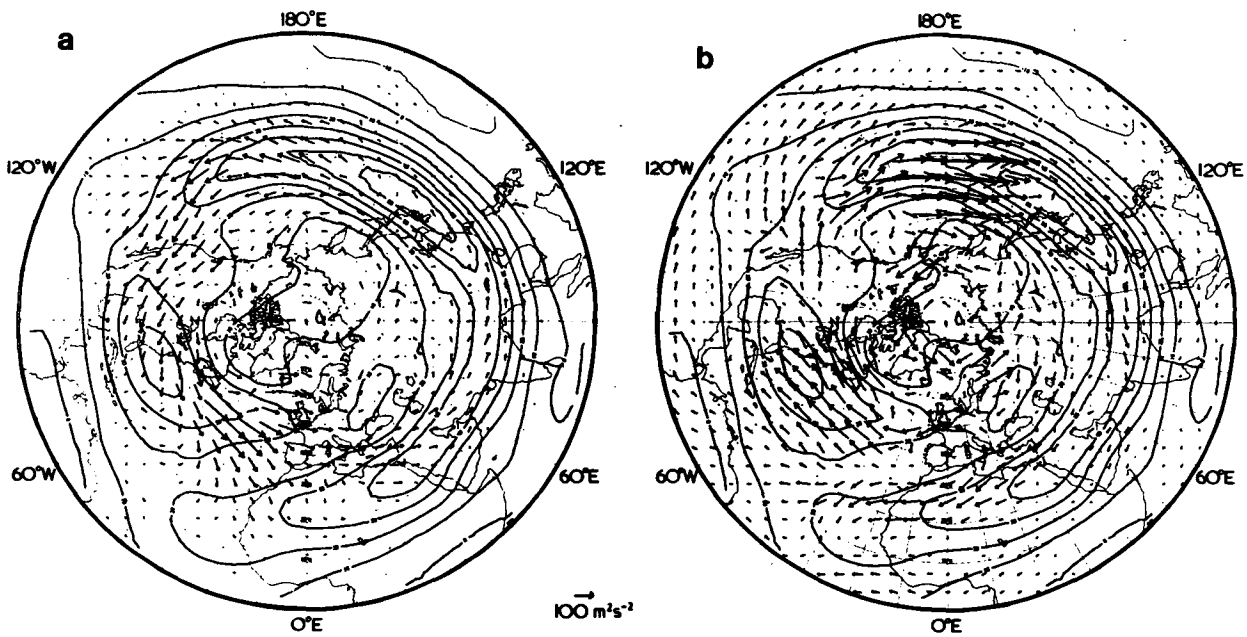

FIG. 6. The 'vector' $\mathbf{E} = (\overline{v'^2 - u'^2}, -\overline{u'v'})$ at 250 mb for the Northern Hemisphere (1979–80 winter, together with contours of $\bar{u}$. The contour interval is 10 m s^{-1}, with maximum values just south of Japan slightly in excess of 60 m s^{-1}, and weak easterlies (around 10 m s^{-1}) in the tropical western Pacific. (a) High-pass eddies; (b) Low-pass eddies. The maximum value of $|\mathbf{E}|$, in the central Pacific in (b) is 430 m^2 s^{-2}.

wave activity moving eastwards at a speed less than that of the mean flow.

Plots of **E** therefore provide a simple way of summarising the eddy feedback onto the mean flow as well as the eddy anisotropy and group velocity characteristics. However, in going from the tensor components M and N to **E**, approximations have been made in which the x and y directions have been treated differently, so that **E** does not transform as a vector. It could be considered that any of the long storm-track, temperature contour or vorticity contour directions are more fundamental. However it may be shown that if **E** is at an angle ϵ_1 with the x-axis when approximated in one coordinate system then, when approximated relative to a coordinate system rotated by an angle ϵ_2, the magnitude and direction of **E** are changed by order the maximum of ϵ_2^2 and $\epsilon_1\epsilon_2$. Thus, for coordinate and **E** directions not differing too much from the zonal direction, the change in **E** is small. An example in which this is checked will be given below.

4. Quasi-geostrophic baroclinic theory

It is often preferable to consider the mechanical and thermal effects of the eddies separately, in particular because the vorticity flux alone influences the depth averaged vorticity balance. However, it is also of interest to extend the above theory to the quasi-geostrophic, baroclinic case.

For simplicity we shall make the Boussinesq approximation and use as thermodynamic variable a buoyancy b which may be considered to be $g[\theta - \Theta(z)]/\theta_0$ where θ is the potential temperature, $\Theta(z)$ a standard distribution and θ_0 a standard value. The thermal wind relations are

$$f_0 u_z = -b_y, \quad f_0 v_z = b_x,$$

and the quasi-geostrophic potential vorticity equation is

$$(\partial_t + \mathbf{v}\cdot\nabla)q = \mathcal{D}, \tag{29}$$

where $q = \zeta + f_0(b/\mathcal{N}^2)_z$ and $\mathcal{N}^2(z)$ is the square of the basic buoyancy frequency. The local dispersion relation for waves of the form $\cos(kx + ly + mz - \omega t)$ is

$$\omega = k\bar{u} + l\bar{v} - (k^2 + l^2 + f_0^2 m^2/\mathcal{N}^2)^{-1}(k\bar{q}_y - l\bar{q}_x). \tag{30}$$

Defining the group velocity $\mathbf{c} = (\partial\omega/\partial k, \partial\omega/\partial l, \partial\omega/\partial m)$, and proceeding as in Section 2 gives

$$\tfrac{1}{2}\overline{q'^2}(\mathbf{c}_g - \bar{\mathbf{v}}) = |\nabla\bar{q}|(-\tilde{M} - \tfrac{1}{2}\overline{b'^2}/\mathcal{N}^2, -\tilde{N}, f_0\overline{v'b'}/\mathcal{N}^2), \tag{31}$$

where the tilde axes are tangential and normal to $\bar{q}$ contours. The extra ingredients added by the baroclinicity are a component westwards along $\bar{q}$ contours proportional to the buoyancy (or temperature) variance, and a vertical component proportional to the cross $\bar{q}$ heat flux. Typical magnitudes of $-\tfrac{1}{2}\overline{b'^2}/\mathcal{N}^2$ for the high-pass eddies are -50 m^2 s^{-2} in the lower troposphere and -20 m^2 s^{-2} near the 250 mb level. The lower tropospheric values are comparable with $\tilde{M}$ so that, qualitatively, the 'eastwards' component of the group velocity may be expected to be comparable with that of the mean flow. At upper levels the baroclinic component merely implies some reduction in the excess of the group velocity over the mean flow speed, The comparable values for the low-pass eddies are -100 m^2 s^{-2} and -50 m^2 s^{-2}, but the baroclinic component now acts only to increase the notion that the group velocity is westwards relative to the mean flow.

The eddy potential enstrophy equation is

$$(\partial_t + \bar{\mathbf{v}}\cdot\nabla)\tfrac{1}{2}\overline{q'^2} + \overline{\mathbf{v}'q'}\cdot\nabla\bar{q} = \overline{\mathcal{D}'q'} \tag{32}$$

Now

$$\begin{aligned}\overline{\mathbf{v}'q'} &= \overline{\mathbf{v}'\zeta' + f_0\mathbf{v}'(b'/\mathcal{N}^2)_z} \\ &= [-M_y + N_x + f_0(\overline{u'b'}/\mathcal{N}^2)_z, \\ &\quad -M_x - N_y + f_0(\overline{v'b'}/\mathcal{N}^2)_z] \\ &\quad + \frac{1}{\mathcal{N}^2}[(\tfrac{1}{2}\overline{b'^2})_y, -(\tfrac{1}{2}\overline{b'^2})_x].\end{aligned} \tag{33}$$

As before, with the stringent assumption that horizontal gradients of mean flow quantities may be neglected compared with those of eddy fluxes, (33) and (31) give

$$\overline{\mathbf{v}'q'}\cdot\nabla\bar{q} = \nabla_3\cdot[(\mathbf{c}_g - \bar{\mathbf{v}})\tfrac{1}{2}\overline{q'^2}]. \tag{34}$$

Here ∇_3 is the three-dimensional gradient operator. Since $\bar{\mathbf{v}}$ is horizontal and non-divergent, (34) substituted in (32) gives a conservation relation for the eddy potential enstrophy:

$$\partial_t\tfrac{1}{2}\overline{q'^2} + \nabla_3\cdot(\mathbf{c}_g\tfrac{1}{2}\overline{q'^2}) = \overline{\mathcal{D}'q'}. \tag{35}$$

Again this is the result of Young and Rhines (1980). Recently Andrews (1983) has derived a conservation relation for quasi-geostrophic eddies which also applies in three space dimensions. His derivation does not require such a restrictive assumption but does require the eddies to be of small amplitude. Also, the final form of the relation is somewhat complicated since the flux term itself includes time derivatives. The relative usefulness of the results of Young and Rhines (1980) and Andrews (1983) remains to be determined.[3]

[3] Plumb (personal communication, 1983) has also derived a quasi-geostrophic eddy conservation relation in which the flux involves ageostrophic velocities.

The feedback of the eddies onto the mean flow may be seen from the mean potential vorticity equation:

$$(\partial_t + \bar{\mathbf{v}}\cdot\nabla)\bar{q} + \nabla\cdot\overline{\mathbf{v}'q'} = \bar{\mathcal{D}}. \tag{36}$$

From (33), the eddy term may be rewritten

$$\nabla\cdot\overline{\mathbf{v}'q'} = \partial_y\nabla_3\cdot(-2M, -N, f_0\overline{v'b'}/\mathcal{N}^2) + \partial_x\nabla_3\cdot(N, 0, f_0\overline{u'b'}/\mathcal{N}^2). \tag{37}$$

The convergence associated with the x-component of "heat" flux is generally negligible compared with that associated with the y-component. The smallness of the horizontal component contribution to the last term in (37) was discussed in Section 3, and so it may be anticipated that the whole term may be neglected. This gives

$$\nabla\cdot\overline{\mathbf{v}'q'} \approx \partial_y\nabla_3\cdot\mathbf{E}. \tag{38}$$

This is the three-dimensional version of (26) where the three-dimensional "vector" $\mathbf{E}$ is now defined as

$$\mathbf{E} = (\overline{v'^2 - u'^2}, -\overline{u'v'}, f_0\overline{v'b'}/\mathcal{N}^2). \tag{39a}$$

In pressure coordinates we would have

$$\mathbf{E} = (\overline{v'^2 - u'^2}, -\overline{u'v'}, f_0\overline{v'\theta'}/\Theta_p). \tag{39b}$$

It is noteworthy that the last two components are, for zonal averaging, identical with those of the Eliassen–Palm flux.

A complete mathematical problem for the mean flow is given by the potential vorticity equation (36) and boundary conditions. On a lower boundary on which $w = 0$, the mean thermodynamic equation is

$$(\partial_t + \bar{\mathbf{v}}\cdot\nabla)\bar{b} + \nabla\cdot\overline{\mathbf{v}'b'} = \bar{Q}. \tag{40}$$

Thus the total effect of the eddies is given by $\mathbf{E}$ through its relation (38) with the potential vorticity flux divergence and its vertical component at a lower boundary, provided again that $\nabla\cdot\overline{\mathbf{v}'b'}$ in (40) is dominated by $\partial_y\overline{v'b'}$.

Since the mean potential vorticity is $\bar{q} = f + \bar{v}_x - \bar{u}_y + f_0(\bar{b}/\mathcal{N}^2)_z$, again the mean flow forcing in the free atmosphere is the same as if there was an eddy x-momentum flux

$$-\mathbf{E} = (\overline{u'^2 - v'^2}, \overline{u'v'}, -f_0\overline{v'b'}/\mathcal{N}^2). \tag{41}$$

Just as the extra horizontal term $-\overline{v'^2}$ may be associated with the y component of the mean horizontal ageostrophic circulation $f_0^{-1}[-(\overline{v'^2})_y, (\overline{v'^2})_y, 0]$ whose x component would tend to balance the y-momentum equation, so the vertical component may be associated with the y-component of the mean vertical ageostrophic circulation $[0, (\overline{v'b'}/\mathcal{N}^2)_z, -(\overline{v'b'}/\mathcal{N}^2)_y]$ whose vertical component would tend to balance the thermodynamic equation. A direct approach revealing the importance of $\nabla_3\cdot\mathbf{E}$ in the x-momentum equation is given in Appendix A.

If the boundary condition (40) is incorporated in terms of a δ-function in potential vorticity in the manner of Bretherton (1966), then it may be seen that a boundary positive meridional heat flux implies an upward component of $\mathbf{E}$, a δ-function divergence below it, and acts in the same way as a positive δ-function forcing of westerly momentum at the surface. However, this way of viewing the problem tends to overemphasize the role of eddy heat flux. Ageostrophic vertical circulations distribute the boundary δ-function westerly forcing over a scale height depth, thus giving a large cancellation with the easterly forcing implied by the convergence of $\mathbf{E}$ in the middle and upper troposphere. Consequently it is often preferable to consider separately the mean barotropic and baroclinic forcings associated with the horizontal and vertical components of $\mathbf{E}$, respectively.

Just as the horizontal components of $\mathbf{E}$ describe the characteristic horizontal eddy shape, so the vertical component gives a measure of the characteristic westward tilt with height. Further, although the information is largely qualitative, comparison of (39a) with (31) shows that $\mathbf{E}$ gives an indication of the vertical as well as horizontal propagation of the eddy activity when such notions are valid.

The heat flux by transient eddies is a maximum at lower tropospheric levels so that a quite complete picture of eddy structure, group velocity and mean flow forcing may be obtained by plotting contours of low level poleward heat flux along with arrows showing the horizontal portion of $\mathbf{E}$ at an upper tropospheric level. Fig. 7 shows such pictures for the high- and low-pass transient eddies in the Northern Hemisphere 1979–80 winter. As demonstrated by the heat flux contours, the high-pass eddies (Fig. 7a) exhibit low-level westward tilt with height, which one may assume is a reflection of their growth through baroclinic processes, and upward propagation of wave activity. At upper levels, as discussed before, meridionally elongated eddy activity propagates downstream and equatorwards. Using the potential vorticity approach to the mean flow problem, the eddies give a forcing equivalent to a westerly δ-function at low levels early in the stormtrack. As Holopainen *et al.* (1982) found, the convergence of the vertical component of $\mathbf{E}$ at upper levels probably dominates the divergence of the horizontal component to give an equivalent of easterly forcing. Further along the storm-track the horizontal convergence of $\mathbf{E}$ implies easterly forcing. However, in the spirit of the above comments, it is somewhat simpler to note the tendency of the eddies to weaken the mean baroclinity and thus the vertical shear in the mean westerly wind and to increase the mean barotropic westerly wind. The former occurs in the beginning of the storm track

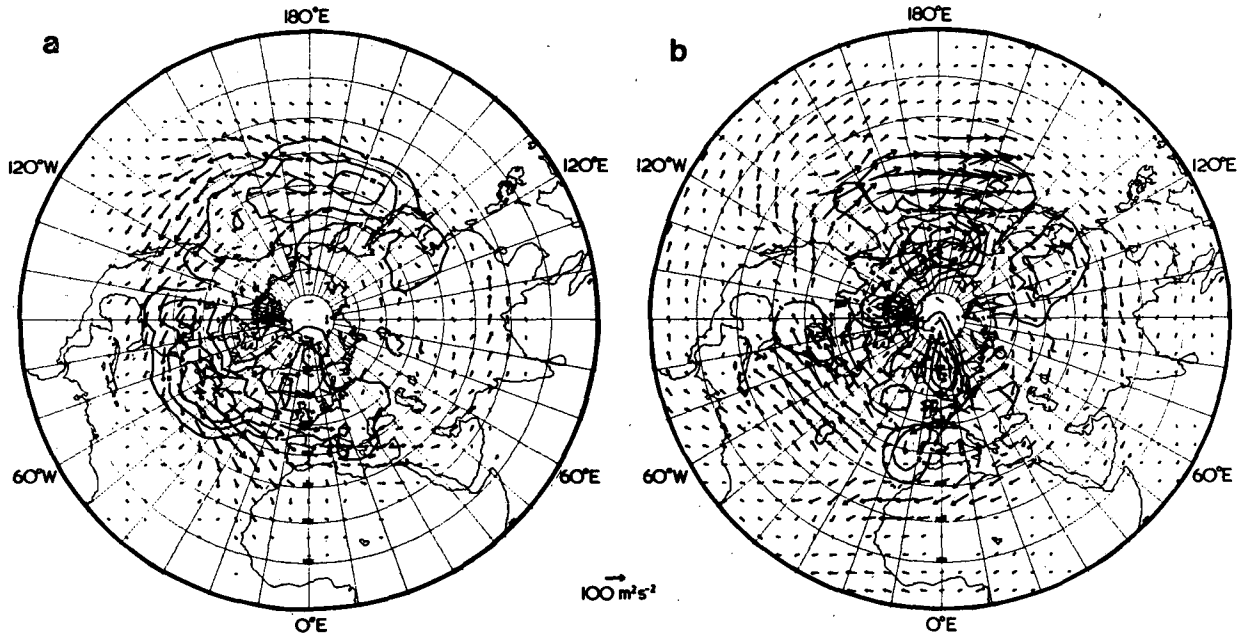

FIG. 7. The three-dimensional pattern of **E** for the Northern Hemisphere 1979–80 winter, indicated by $\mathbf{E} = (\overline{v'^2} - \overline{u'^2}, -\overline{u'v'})$ at 250 mb, together with the poleward temperature flux $\overline{v'T'}$ at 700 mb (contour interval 5 K m s^{-1}; the first contour displayed is for +5 K m s^{-1}). (a) High-pass filtered transients; (b) Low-pass filtered transients.

and the latter in the beginning and middle of the track.

The low-pass eddies at the exits of the Pacific and Atlantic jets (Fig. 7b) show some evidence of low-level baroclinic structure and upward propagation, but display mainly the barotropic picture of zonally elongated eddies propagating slower than the westerly flow. The mean flow forcing has the equivalent of a small westerly δ-function at low levels near 160°E, 35°N. At upper levels, the convergence of the vertical component of **E** reinforces that of the horizontal component to give strong easterly forcing. Near 160°W the divergence of the horizontal components of **E** implies westerly forcing, as before. Again, an easier interpretation is perhaps provided by observing the tendency to reduce the vertical shear in the westerly wind near 160°E and decrease the barotropic westerlies there and to increase the barotropic westerlies near 160°W.

Finally, returning to the approximations made in the theory developed here, it should be noted that the vertical component of **E**, like the horizontal components, depends on the orientation of the axes used. One might anticipate however that for a heat flux dominated by its meridional component there will be only small sensitivity to small rotations of the x-axis from the zonal direction. As an example, Fig. 8 shows the high-pass transient eddy picture corresponding to Fig. 7a except that **E** is determined locally using the 250 mb streamfunction contours shown in Fig. 1.

The differences are nearly all small, and are most pronounced in the diffluent part of the flow in the mid-Atlantic (around 20–30°W), where the streamlines make fairly large angles with the zonal direction.

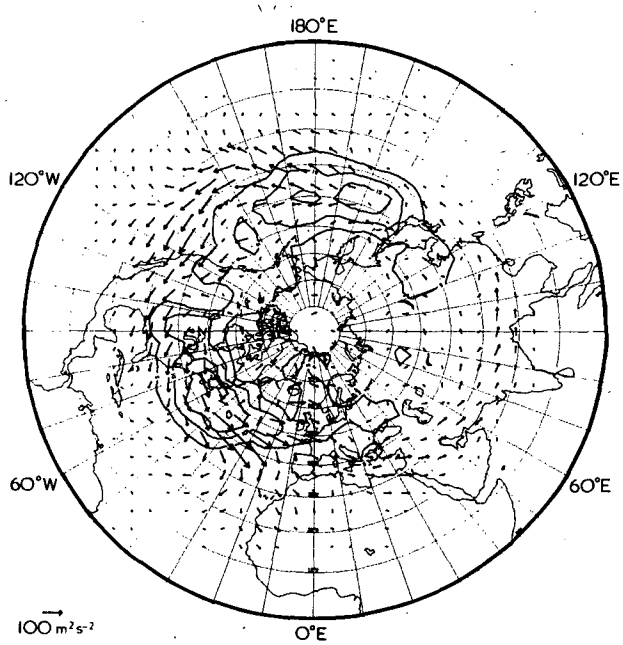

FIG. 8. As in Fig. 7a, except that **E** and $\overline{v'T'}$ are determined relative to local coordinates aligned with contours of $\bar{\psi}$ at 250 mb (see Fig. 1).

In particular, the equatorward turning of **E** at the southeast end of the storm track is accentuated. However, the pattern of $\nabla \cdot \mathbf{E}$ is virtually unaltered by the rotation, since the vectors are quite small in the regions where they are rotated through large angles. It is found that the low-pass pictures show agreement in the important jet exit regions but differ over Europe and near 170°E, 60°N and 60°W, 60°N where, again, the orientation of the streamfunction contours is less zonal. In the regions in which eddy forcing of the mean flow is important and has been discussed in this paper, **E** appears to be almost invariant under the small horizontal rotations of coordinate systems which are generally relevant. Therefore, the usual latitude-longitude system may be used for evaluation.

5. Some comments on the Southern Hemisphere circulation

The ECMWF archives are global, and while the Southern Hemisphere analyses are undoubtedly of substantially poorer quality than those of the Northern Hemisphere, it seems worth applying the above ideas to them. Accordingly, some Southern Hemisphere pictures are now presented for the period 1 June 1980 to 31 August 1980. The results broadly confirm and extend the findings of Physick (1981) and Trenberth (1981, 1982). The mean flow is shown in Fig. 9. The jet is rather uniform, but with a weaker section in the east Pacific, and an upper level maximum west of Australia. There is a slight split of the jet to the south of Australia.

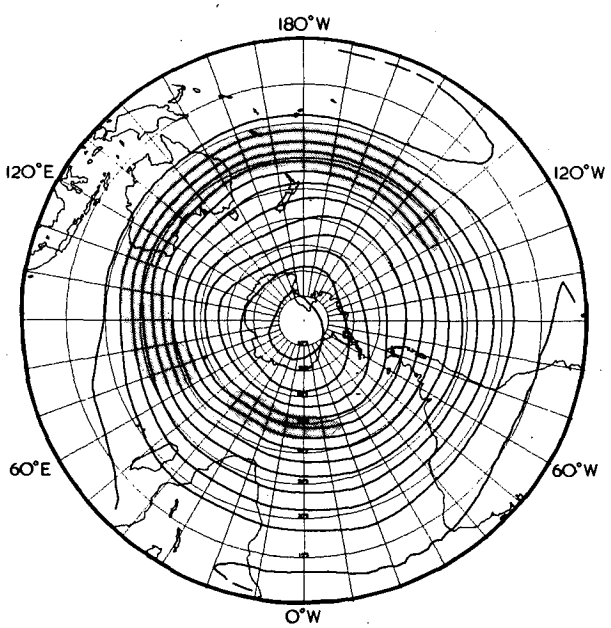

FIG. 9. Contours of $\bar{\psi}$ at 250 mb for the Southern Hemisphere from 1 June 1980 to 31 August 1980. Contour interval is 12.7 $\times 10^6$ m^2 s^{-1}, as in Fig. 1. The shading indicates wind speeds higher than 35 m s^{-1}. The largest wind speeds, somewhat less than 50 m s^{-1}, were over the Pacific Ocean north of New Zealand.

The high- and low-pass filtered velocity correlation tensor is illustrated by Fig. 10. The high-pass filtered correlations reveal a single extended region of enhanced eddy activity starting in the mid-Atlantic and coming to an end near Australia. The anisotropy index $\alpha = \hat{M}/K$, is generally near 0.5 throughout the storm track, a value rather larger than in the Northern Hemisphere. The high frequency eddies are again characteristically extended in the meridional direction.

The low frequency eddies are much weaker than their Northern Hemisphere counterparts. The maxima, both of K and $\hat{M}$, tend to be localized, with the most intense maximum at 100°E, 35°S. Here and elsewhere, the eddy axes are zonally directed. An exception is the region of the Drake passage where $\overline{v'^2}$ exceeds $\overline{u'^2}$ and so the anisotropy index is large, between 0.5 and 0.6, in the neighborhood of the maxima in K.

The two dimensional **E** vector is a very good approximation to the eddy propagation and mean flow forcing indicated by the eddy anisotropy vector. The horizontal components of **E**, shown in Fig. 11, are either normal to the anisotropy vectors (in the case of the high frequency fields), or parallel to them (as for the low frequency eddies). The only region where this is not true is to the west of the Australian continent, where the **E** vectors make very large angles with the zonal direction. Here **E** is more nearly perpendicular to the local anisotropy if it is calculated relative to axes parallel to the local 700 mb isotherm, although the change is rather slight.

The forcing of the mean flow by the eddies is demonstrated in Fig. 12, which shows the exact form of the streamfunction forcing, $S = -\nabla^{-2}(N_{xx} - N_{yy} - 2M_{xy})$. In the Southern Hemisphere, the approximate version $S \approx -\nabla^{-2}(-N_{yy} - 2M_{xy})$ is very similar for both the high and low frequency data. The amplitude of some major features changes slightly, but the shape of the field is not sensitive to the approximation. This close agreement is related to the generally rather slow zonal variation of the Southern Hemisphere flow.

Consistent with Fig. 12, the high-pass filtered **E** vector in Fig. 11a indicates westerly acceleration at 50°S, from 30°E to 130°E, and a corresponding easterly acceleration near 30°S. The associated low level $\overline{v'T'}$ indicates the baroclinic nature of the eddies. The westerly acceleration is particularly intense, reaching values of about 9 m s^{-1} day^{-1} near 55°S, 70°E. At this location, the tendency to accelerate westerlies is also supported by the low-pass filtered transients; it is interesting to note that the tendency of the tropospheric jet to split is particularly marked at this longitude (see Fig. 10). Wave activity propagates into the strong upper level jet over Australia, while low

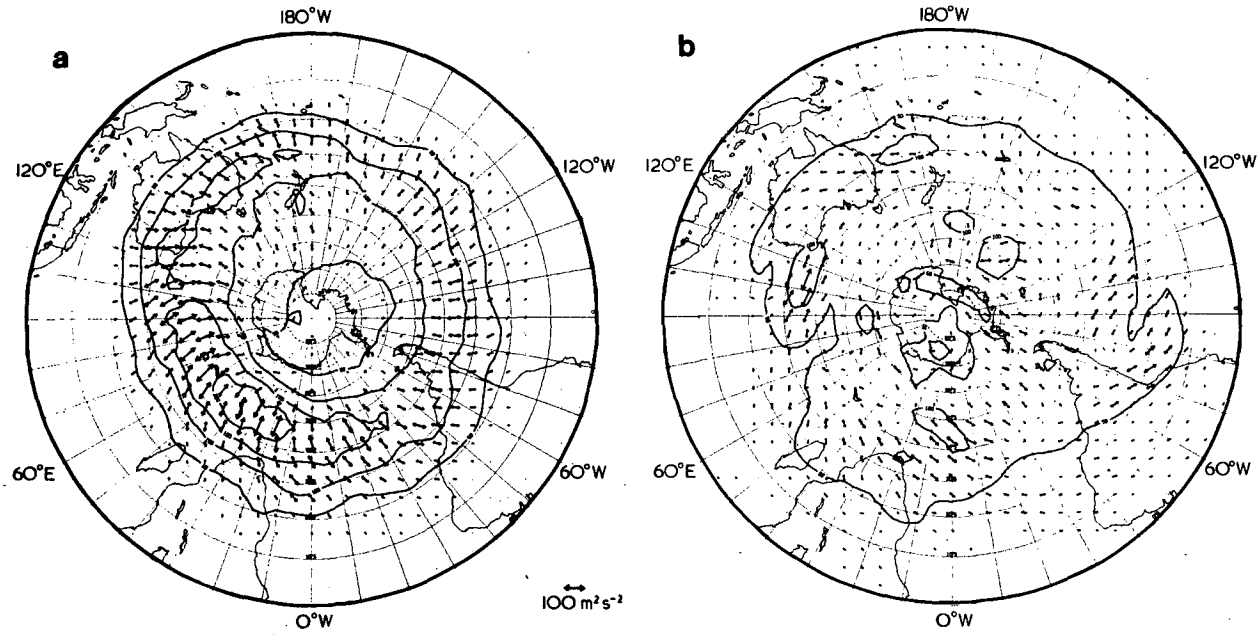

FIG. 10. Illustrating the velocity correlation tensor for (a) high-pass filtered eddies, (b) low-pass filtered eddies for the Southern Hemisphere winter 1980. All other details as for Fig. 2. The high-pass data reveal a single storm track over the southern Atlantic and Indian Oceans, and less eddy activity over the Pacific Ocean. The eddies are elongated meridionally, with a large anisotropy index. In contrast the low-pass eddies are very weak (compare Fig. 3) and rather disorganized.

level baroclinic activity is maintained beneath the southern branch of the jet.

Such data suggest that the well-known propensity of the Southern Hemisphere tropospheric jet to split is strongly supported by transient eddy fluxes of vorticity.

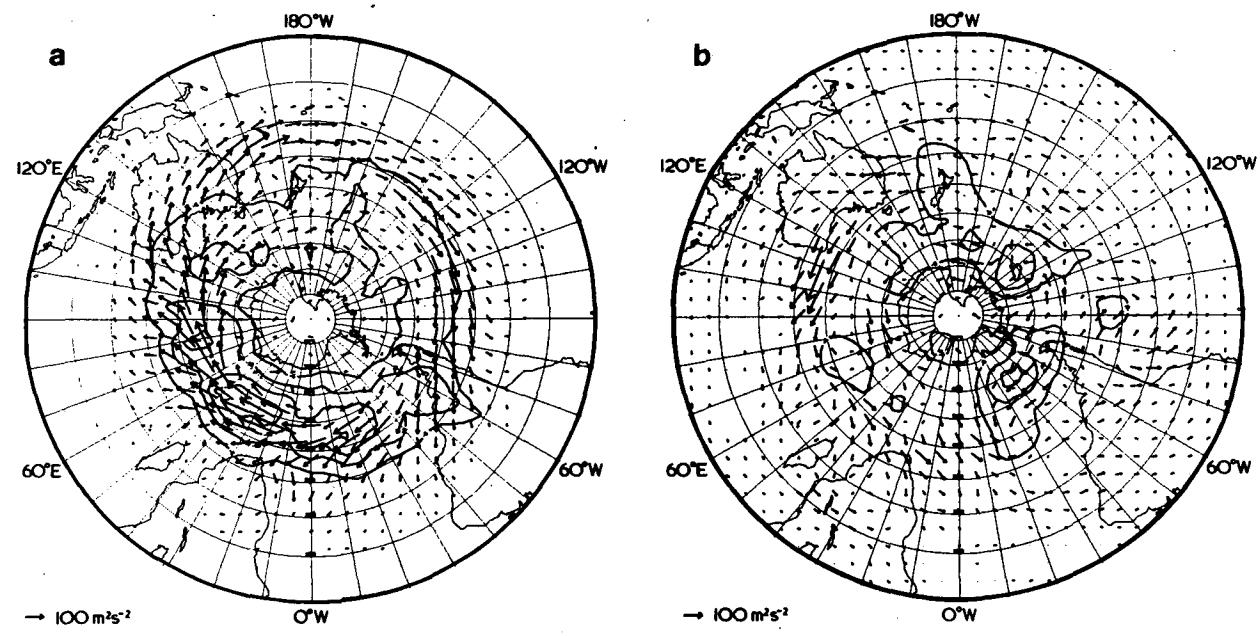

FIG. 11. $\mathbf{E} = (\overline{v'^2 - u'^2}, -\overline{u'v'})$ at 250 mb, together with contours of $\overline{v'T'}$ at 700 mb for the Southern Hemisphere winter 1980. Contour interval is 5 K m s^{-1}, and the first contour plotted is -5 K m s^{-1}. (a) The high-pass filtered eddies show a single storm track over the South Atlantic and Indian Oceans with weaker eddy activity over the Pacific. **E** is generally directed to the east. (b) The low-pass filtered **E** is mostly weak and disorganized with rather little coherent vertical component.

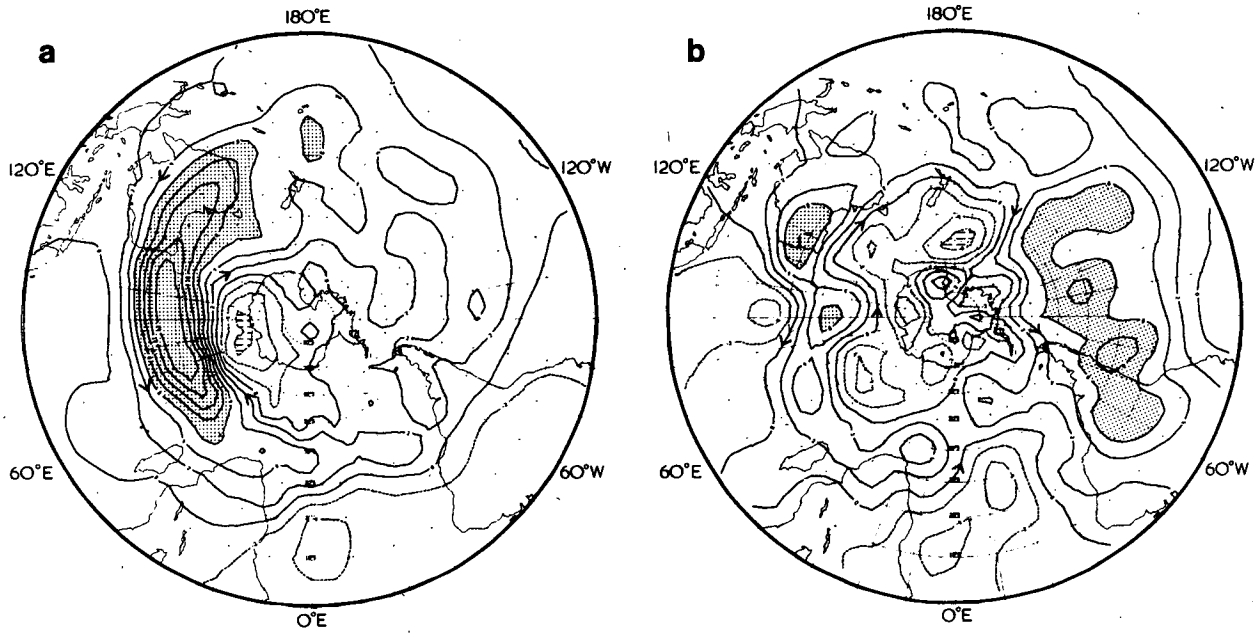

FIG. 12. $S = -\nabla^{-2}(\nabla \cdot \mathbf{v}'\zeta')$ for the Southern Hemisphere winter 1980 at 250 mb. Details are as in Fig. 5. (a) High-pass filtered transients; (b) Low-pass filtered transients. The low-pass S is much less important than in the Northern Hemisphere winter. The zonal variation is relatively small in both the high and low pass fields. The fields are almost unaltered when the approximation $\nabla \cdot \overline{\mathbf{v}'\zeta'} = \partial_y \nabla \cdot \mathbf{E}$ is employed.

A single season of data is not a long enough record from which statistically significant details of the climatology of the low frequency transients can be inferred. The weak, disorganized nature of the field, and barotropic nature of the strongest transients, is however clear from Fig. 11b. Generally, the low frequency transients tend to force westerlies between 40°S and 60°S, and easterlies at more tropical latitudes. A complex quadrupole pattern of forcing (Fig. 12) is associated with the strongest pattern of low frequency **E** vectors to the southwest of Australia.

6. Conclusion

It has been shown that, in simple situations, the anisotropic eddy horizontal velocity correlation tensor implies the shape and propagation of eddies and the feedback of the eddies onto the mean flow. Making an approximation which has been found to be justified in most areas of interest, the diagnostic quantity has been reduced to a "vector" $\mathbf{E} = (\overline{v'^2} - \overline{u'^2}, -\overline{u'v'}, f_0\overline{v'\theta'}/\Theta_p)$. Because of its connection with previous theory, **E** might be referred to as an

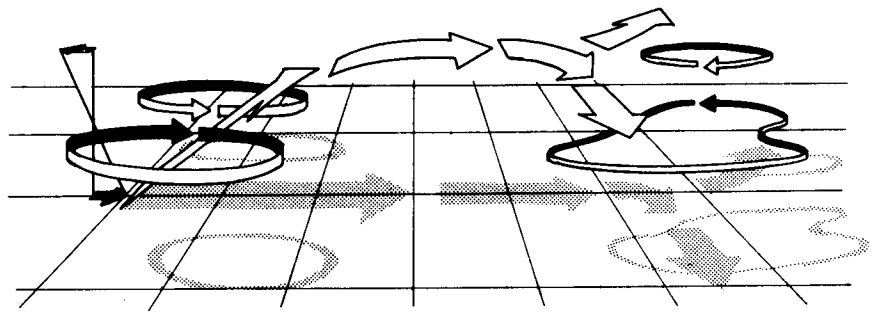

FIG. 13. A schematic diagram of the three-dimensional distribution of **E** for the high-pass filtered eddies in a storm track. Eddy activity originates at low levels at the start of the storm track and propagates upwards and eastwards, where the eddies strengthen the barotropic wind but weaken the vertical wind shear. Towards the end of the storm track eddy activity propagates mainly horizontally in the upper troposphere, with a stronger meridional component, resulting in a slight weakening of the barotropic flow. The feedbacks onto the mean flow are indicated by the negative $\partial\bar{u}/\partial z$ and horizontal circulation arrows.

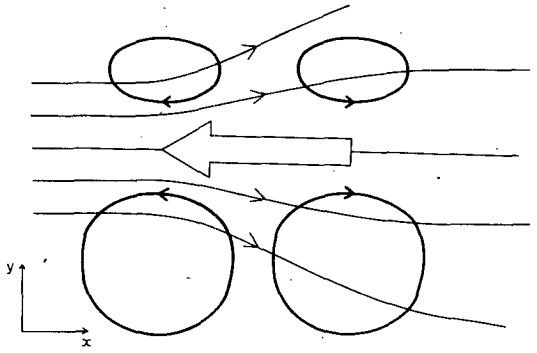

FIG. 14. A schematic diagram of the distribution of **E** for the low-pass filtered eddies in the Northern Hemisphere. The vertical component is insignificant. In the jet exit region, low frequency eddy activity elongated in the zonal direction propagates westwards relative to the mean flow. The resulting mean flow forcing indicated by circulation arrows tends to attenuate the zonal asymmetry of the jet.

extended Eliassen–Palm flux, though it must be recognised that the present three dimensional theory necessitates approximations which were not required in the zonally averaged development of Andrews and McIntyre (1976). Further, the group velocity information given by **E** is essentially qualitative, and **E** plays no direct role in a general eddy conservation relation. Its major quantitative significance is in determining the eddy feedback onto the mean flow. The importance of the zonal or meridional extension of eddies when they occupy a region of limited zonal extent is illustrated through **E** and combined with the more frequently discussed tilted trough momentum flux.

The eddy pictures for the 1979–80 Northern Hemisphere winter have emphasized that, even though there is no gap in the energy spectrum, there is a dramatic change in eddy structure and mean flow feedback near periods of ten days. The high-pass eddies in their storm tracks have a behavior which is summarized in Fig. 13. The main features are low-level baroclinic development and upward propagation followed by downstream and then equatorward propagation of meridionally elongated eddies which develop troughs tilted from SW–NE. The feedback onto the mean flow is in the sense of decreasing the vertical shear in the westerly wind near the entrance to the storm track and increasing the barotropic westerly flow near the entrance and middle of the track. The most important feature in the low-pass eddy pictures is the barotropic behavior in the jet exit regions. This is summarized in Fig. 14. The zonally elongated eddies move westward relative to the zonal flow. Their mean flow forcing is in the sense of reducing the westerly wind where it is strong and increasing it where it is weak. This acts to decrease the kinetic energy of the mean flow and therefore in the absence of dissipation would increase the kinetic energy of the transients. To make this explicit, we note that taking the mean frictionless barotropic vorticity equation with the eddy forcing represented by $-\partial_y \nabla \cdot \mathbf{E}$, multiplying by $\bar{\psi}$ and integrating over the globe using integration by parts gives

$$d/dt \text{ (eddy kinetic energy)}$$
$$= -d/dt \text{ (mean kinetic energy)}$$
$$= -\text{correlation of } \bar{u} \text{ and } \nabla \cdot \mathbf{E}.$$

This is entirely consistent with the study of Simmons *et al.* (1983) which shows that typical time mean upper tropospheric flows are barotropically unstable to perturbations which during their time of maximum

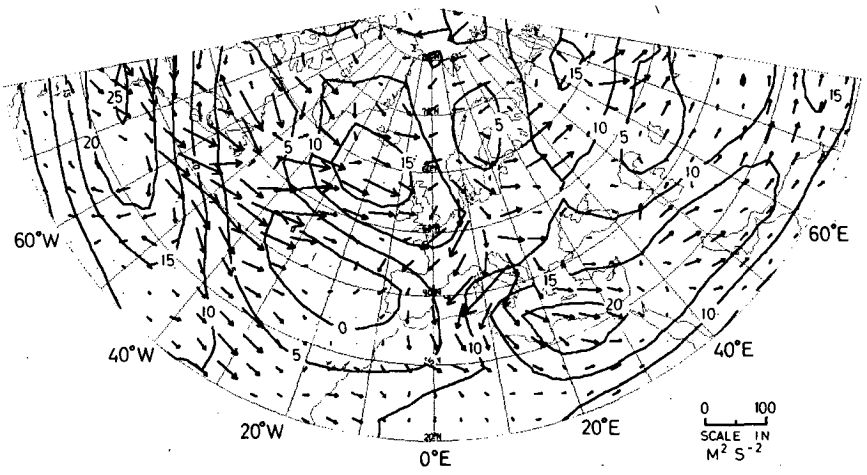

FIG. 15. The barotropic flow and **E** vector during a North Atlantic blocking episode. Contours show $\bar{u}$ (contour interval 5 m s^{-1}) and the vectors the high-pass filtered $\mathbf{E} = (\overline{v'^2} - \overline{u'^2}, -\overline{u'v'})$, both averaged between 1000 mb and 150 mb, for the period 26 November–7 December 1981. Note the tendency for the transient forcing to reinforce the block.

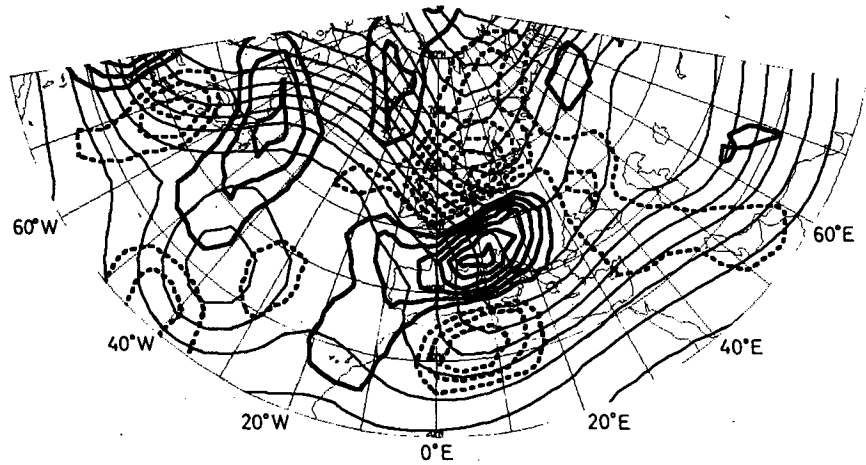

FIG. 16. The form of the slowly and rapidly varying components of the 250 mb geopotential height on 4 December 1981 during the block shown in Fig. 14. The heavy contours drawn every 10 m indicate the high frequency transients, solid contours being positive and dashed negative. The mean field and low frequency transients are shown by the light contours, the interval being 100 m. Details of the calculation are given in the text. Upstream of the block the eddies are oriented north–south, while downsteam they are extended in the east–west direction.

amplitude have exactly the structure shown in Fig. 14. Fig. 16 of Simmons *et al.* shows the horizontal extended Eliassen–Palm flux picture for a typical mode and is strikingly similar to the real data picture shown in Fig. 6b. There are signs in the full picture (Fig. 7b) that the baroclinic structure of these eddies might be of some importance. Finally, we note that the zonal extent of large $\overline{u'^2}$ is only about 40°. Since the eddies are elongated in this zonal direction, this is suggestive that the **E** vector signature is that of a standing oscillation in the jet exit region corresponding to the large or small extension of the Asian jet over the Pacific.

The **E** vector can also play a useful role in investigating the feedback of transient eddies of synoptic time scales onto low-frequency atmospheric behavior such as blocking. The period 26 November–7 December 1981 was characterized by a blocking high in the eastern Atlantic. The time-mean zonal wind for that period, vertically averaged between 1000 and 150 mb, is displayed in Fig. 15, together with the vertically averaged **E** vector for high-pass filtered transients. [The particular high-pass filter used has a cut-off of approximately 7 days; it is described on pages 7–9 of Lau *et al.* (1981).] The vectors both upstream and downstream of the block tend to point towards the region of weak flow, implying a convergence of **E** and an easterly acceleration of the mean flow there, thus tending to maintain the block. An example of the structure of the synoptic eddies which produce such a pattern is shown in Fig. 16, which contrasts low- and high-frequency components of 250 mb geopotential height for 3–5 December 1981. The low-frequency component was obtained by a +1+2+1 weighting of the three daily height fields and is shown by the lighter contours. The block is clearly evident. The heavier contours show the high-frequency component, obtained by a −1+2−1 weighting of the three height fields. The changing orientation of high-frequency disturbances as they move around the block, and the resulting change in the **E** vector is clearly evident and agrees with synoptic experience. As systems approach the block from the west they become meridionally elongated and weaken. On the east side of the block cold air outbreaks from the north are associated with zonally elongated transients. Further case studies of blocking episodes are planned.

Acknowledgments. The development of the ideas described here was greatly aided by many fruitful hours of discussion with Dr. J. M. Wallace. The comments of Dr. D. G. Andrews, Dr. R. A. Plumb and Dr. J. R. Holton have helped clarify the presentation. The important contribution of Dr. J. S. A. Green to Appendix A was most welcome. We are grateful to the staff of ECMWF for their cooperation and advice in compiling diagnostics from their archives, and to the U.K. Meteorological Office who made computing facilities at ECMWF available to us. Dr. M. A. Pedder introduced us to the Lanczos filter.

APPENDIX A

An Alternative Approach Using the Mean-Flow Momentum Equations

For simplicity, consider the mean vector horizontal momentum equation on an f-plane:

$$\bar{D}\bar{\mathbf{v}} = -f\mathbf{k} \times \bar{\mathbf{v}}_a + \mathbf{V}, \qquad \text{(A1)}$$

where

$$\bar{\mathbf{v}}_a = \bar{\mathbf{v}} - f^{-1}\mathbf{k} \times \nabla\bar{\phi},$$

$$\mathbf{V} = -(\nabla \cdot \overline{\mathbf{v}'u'}, \nabla \cdot \overline{\mathbf{v}'v'}),$$

and ∇ is the horizontal gradient operator. The convergence of the eddy vertical flux of momentum has been neglected. The curl of $\mathbf{V}$ forces mean vorticity whilst its divergence enters only in the mean divergence equation which in most large-scale situations reduces to the balance equation. Therefore we may consider defining a modified mean ageostrophic velocity and a modified eddy momentum flux convergence:

$$\bar{\mathbf{v}}_{am} = \bar{\mathbf{v}} - f^{-1}\mathbf{k} \times \nabla(\bar{\phi} + S), \tag{A2}$$

$$\mathbf{V}_m = -(\nabla \cdot \overline{\mathbf{v}'u'}, \nabla \cdot \overline{\mathbf{v}'v'}) + \nabla S. \tag{A3}$$

The momentum equation with these modified definitions is identical in form with (A1) and $\nabla \cdot \bar{\mathbf{v}}_{am} = \nabla \cdot \bar{\mathbf{v}}_a$.

As suggested by J. S. A. Green (personal communication, 1982) it is natural to choose S to minimize the almost irrelevant divergence of $\mathbf{V}_m$. This can also be shown (J. S. A. Green) to be the condition that the rms length of $\mathbf{V}_m$ be minimized. Now

$$\nabla \cdot \mathbf{V}_m = -(\overline{u'^2})_{xx} - 2(\overline{u'v'})_{xy} - (\overline{v'^2})_{yy} + S_{xx} + S_{yy}, \tag{A4}$$

$$\mathbf{k} \cdot \nabla \times \mathbf{V}_m = (\overline{u'^2 - v'^2})_{xy} - (\overline{u'v'})_{xx} - (\overline{u'v'})_{yy}. \tag{A5}$$

For the synoptic time-scale eddies, $\overline{v'^2}$ is larger than $\overline{u'^2}$ and $\overline{u'v'}$, and $\partial/\partial y \gg \partial/\partial x$. Thus (A4) suggests that a choice $S = \overline{v'^2}$ will reduce the divergence of $\mathbf{V}_m$ and make it much smaller than its curl. For the longer time-scales, with $\overline{u'^2}$ dominating and $\partial/\partial y \gg \partial/\partial x$, the divergence is smaller than the curl even with $S = 0$. However, the choice $S = \overline{v'^2}$ maintains their relative magnitudes.

Choosing $S = \overline{v'^2}$, (A2) and (A3) give

$$\bar{\mathbf{v}}_{am} = \bar{\mathbf{v}} - f^{-1}\mathbf{k} \times \nabla(\bar{\phi} + \overline{v'^2}), \tag{A6}$$

$$\mathbf{V}_m = (\nabla \cdot \mathbf{E}, -(\overline{u'v'})_x), \tag{A7}$$

where $\mathbf{E}$ is defined as in (26). The scalar momentum equations are therefore

$$D\bar{u} = f\bar{v}_{am} + \nabla \cdot \mathbf{E}, \tag{A8}$$

$$D\bar{v} = -f\bar{u}_{am} - (\overline{u'v'})_x. \tag{A9}$$

The eddy forcing term $-(\overline{u'v'})_x$ in (A9) is generally very small so that the mechanical forcing by the eddies is accurately represented by $\nabla \cdot \mathbf{E}$ in the x-momentum equation.

In three dimensions at the level of quasi-geostrophic theory, the mean equations of motion for a Boussinesq, adiabatic fluid may be written:

$$\left.\begin{aligned} D\bar{u} &= f\bar{v} - \bar{\phi}_x - \nabla \cdot (\overline{\mathbf{v}'u'}) \\ D\bar{v} &= f\bar{u} - \bar{\phi}_y - \nabla \cdot (\overline{\mathbf{v}'v'}) \\ D\bar{b} &= -\mathcal{N}^2(z)\bar{w} - \nabla \cdot (\overline{\mathbf{v}'b'}) \end{aligned}\right\}, \tag{A10}$$

with

$$\bar{u}_x + \bar{v}_y + \bar{w}_z = 0 \quad \text{and} \quad \bar{w} = 0 \quad \text{on} \quad z = 0,$$

plus the thermal wind relations involving $\bar{b}$, $\bar{u}$ and $\bar{v}$. Redefining the mean three-dimensional ageostrophic motion:

$$\bar{\mathbf{v}}_{am} = (\bar{u}, \bar{v}, \bar{w}) - f^{-1}\mathbf{k} \times (\bar{\phi} + \overline{v'^2}) + [-(\overline{u'b'}/\mathcal{N}^2)_z, -(\overline{v'b'}/\mathcal{N}^2)_z, \nabla \cdot (\overline{\mathbf{v}'b'})/\mathcal{N}^2], \tag{A11}$$

Eq. (A10) may be written

$$\left.\begin{aligned} D\bar{u} &= f\bar{v}_{am} + \nabla_3 \cdot \mathbf{E} \\ D\bar{v} &= -f\bar{u}_{am} - (\overline{u'v'})_x - f(\overline{u'b'}/\mathcal{N}^2)_z \\ D\bar{b} &= -\mathcal{N}^2\bar{w}_{am} \end{aligned}\right\}, \tag{A12}$$

with

$$\nabla_3 \cdot \bar{\mathbf{v}}_{am} = 0 \text{ and } \bar{w}_{am} = \nabla \cdot (\overline{\mathbf{v}'b'})/\mathcal{N}^2 \text{ on } z = 0.$$

In this form, there is no direct eddy forcing in the $\bar{b}$-equation, usually only very small forcing in the $\bar{v}$-equation, and a forcing in the $\bar{u}$-equation of the form $\nabla_3 \cdot \mathbf{E}$ where $\mathbf{E}$ is the three-dimensional "vector" defined in (39a). The reservation on the utility of this form is that the eddy forcing appears also in the boundary value of $\bar{w}_{am}$. In many respects, (A12) is a natural quasi-geostrophic extension of the transformed mean-flow equations of Andrews and McIntyre (1976) and $\bar{\mathbf{v}}_{am}$ is an extension of their residual circulation concept.

APPENDIX B

Data sources and Manipulation

The data discussed in this paper were extracted from the archives maintained at the European Centre for Medium Range Weather Forecasts (ECMWF). Data is objectively analysed every six hours onto a high resolution latitude–longitude grid and balanced using a normal mode initialization scheme. The multivariate statistical interpolation analysis scheme employed is described by Lorenc (1981); for details of the initialization procedure, see Temperton and Williamson (1981) and Williamson and Temperton (1981). For compact archiving, the fields are expressed as spherical harmonic coefficients (triangular truncation at wavenumber 80), which are then packed so that each word of computer store holds four numbers.

Fields of velocity, temperature, geopotential height, humidity and vertical velocity are archived for 13 standard pressure surfaces distributed approximately logarithmically between 1000 mb and 30 mb. For the purposes of this paper, the 700 mb level was taken to represent the lower troposphere and the 250 mb level the jet stream level. The archives start in September 1979, so that at present climatological statistics of the kind presented by Blackmon *et al.* (1977) and others are not possible. However, statistics for periods as long as complete seasons can be produced easily.

The data extraction programs recover the required fields from the archives, unpack them and calculate gridpoint values for a specified grid. Considerable computer resources can be saved by a careful restriction of the resolution required for the diagnostics. It has proved sufficient to extract data on a 5° latitude–longitude grid, for which only waves up to triangular truncation 30 need be included. Furthermore, rather little variance is associated with periods of less than two days so that the fields need to be extracted only daily when calculating time averages. Since there are few upper air observations at 0600 and 1800 GMT, the model-generated background field will dominate the analysis at these times. In an attempt to maximize the number of observations over the Pacific, the 0000 GMT analyses were used in the present study.

It is believed that the ECMWF analyses are probably the most accurate routine global analyses currently available. But they have a number of readily identifiable shortcomings.

Most seriously, the tropical divergent wind field is seriously attenuated by the initialization procedure. The initialization is nevertheless important away from the tropics, where it removes spurious imbalances beween the mass and wind fields and yields a good estimate of the vertical velocity. The error is related to difficulties in incorporating diabatic processes in the initialization algorithm. Since the discussion in this paper is concerned with mid-latitude effects, the impact of this error can be ignored.

The packing procedure leads to errors in the wind fields at high latitudes (i.e., within 10–15° of the poles). These may be as large as ± 5 m s^{-1}, and some of the noise in the wind variance fields at high latitudes (see, for example, Figs. 5 and 7) may be due to packing errors. This ill-conditioning becomes rapidly less important at lower latitudes and probably is not significant. In polar regions, the split of the wind field into zonal and meridional components, which is crucial to the definition of E, becomes arbitrary. So it may be argued that, because the diagnostic is inappropriate to the polar region, this packing error is unimportant.

It should be recorded that steps have been taken to reduce both these errors, and current ECMWF archives are now more reliable in polar and tropical regions.

Remaining difficulties concern the deficiencies of the observing network itself. Clearly, the analyses will be of poorer quality in the Southern Hemisphere, in the stratosphere and over the oceans. It is difficult to quantify the uncertainty. However, some of the more glaring shortcomings, such as heat flux maxima centered on Southern Hemisphere island stations noted by earlier workers (van Loon, 1980) are not as apparent. Further discussion of these points is given in White (1982).

Filtering of the transient variance and co-variance fields was accomplished using a 31-point filter, so that the filtered version $\tilde{q}$ of any quantity of q is given by

$$\tilde{q}_t = \sum_{i=-n}^{n} a_i q_{t+i}, \qquad \text{(B1)}$$

where t denotes the time level, a_i are the filter coefficients and $n = 15$ in our case. High and low pass filter coefficients were calculated using the Lanczos method [see Duchon (1979)]. Its advantage lies in the sharpness of the response and the near absence of any Gibbs phenomena around the cut-off frequencies. Clearly such a filter requires a further n time levels at either end of the data sequence, and its implementation will carry a computational penalty. This proved fairly small compared with the cost of an unfiltered calculation for a seasonal sequence. For calculations involving much shorter data sequences, such as that described in Section 6, a simpler filtering technique, based on Lorenz's "poor man's spectral analysis" [Lorenz (1979)] was used.

For the seasonal means described in this paper, a high-pass and a low-pass filter, each with a cut-off

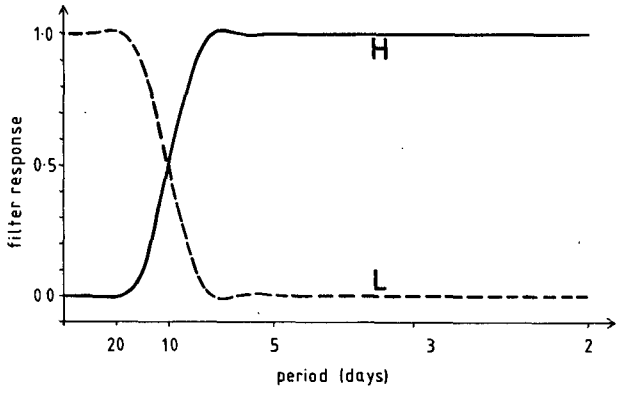

FIG. B1. Response functions of the 31-point Lanczos filters used in this paper. L denotes the low pass filter, with a high frequency cutoff corresponding to a period of 10 days, while H denotes the high pass filter with the low frequency cutoff at a period of 10 days. The L filter passes 19% of the variance of white noise, while the H filter passes 81% of the variance.

period of 10 days, were chosen. The pattern of the filtered fields is insensitive to the precise values of the cut-off, although their magnitudes will change. Life cycle calculations (Simmons and Hoskins (1978)) suggested that periods between 2 and 10 days would include most of the variance directly due to baroclinic instability. The response curves for these filters are shown in Fig. B1.

On a spherical domain, any spatial filtering needed is best done by operating on the spectral coefficients. For example, the large-scale structures present in the vorticity forcing were demonstrated by applying a ∇^{-2} operator on the basic field (Fig. 5). The necessary spectral decomposition was accomplished by using a fast Fourier transform in the zonal direction and by direct numerical integration (using the trapezium rule) in the meridional direction. The resulting spectral coefficients are reasonably accurate, especially if the coefficients for large total wavenumber are to be reduced or set to zero. In the case of a 5° grid, the application of a ∇^{-2} operator required only a second or so of computer time.

REFERENCES

Andrews, D. G., 1983: A conservation law for small-amplitude quasi-geostrophic disturbances on a zonally asymmetric basic flow. *J. Atmos. Sci.*, **40**, 85–90.

——, and M. E. McIntyre, 1976: Planetary waves in horizontal and vertical shear: the generalized Eliassen–Palm relation and the mean zonal acceleration. *J. Atmos. Sci.*, **33**, 2031–2048.

Blackmon, M. L., J. M. Wallace, N.-C. Lau and S. L. Mullen, 1977: An observational study of the Northern Hemisphere wintertime circulation. *J. Atmos. Sci.*, **34**, 1040–1053.

——, Y. H. Lee and J. M. Wallace, 1983: Horizontal structure of 500 mb height fluctuations with short, intermediate and long time scales. *J. Atmos. Sci.*, **40** (in press).

Bretherton, F. P., 1966: Critical layer instability in baroclinic flows. *Quart. J. Roy. Meteor. Soc.*, **92**, 325–334.

Dingle, R. B., 1973: *Asymptotic Expansions: Their Derivation and Interpretation.* Academic Press, 521 pp.

Duchon, C. E., 1979: Lanczos filtering in one and two dimensions. *J. Appl. Meteor.*, **18**, 1016–1022.

Edmon, H. J., B. J. Hoskins and M. E. McIntyre, 1980: Eliassen–Palm cross sections for the troposphere. *J. Atmos. Sci.*, **37**, 2600–2616.

Holopainen, E. O., 1978: On the dynamic forcing of the long-term mean flow by the large-scale Reynolds stresses in the atmosphere. *J. Atmos. Sci.*, **35**, 1596–1604.

——, and A. H. Oort, 1981: On the role of large-scale transient eddies in the maintenance of the vorticity and enstrophy of the time-mean atmospheric flow. *J. Atmos. Sci.*, **38**, 270–280.

——, L. Rontu and N.-C. Lau, 1982: The effect of large-scale transient eddies on the time-mean flow in the atmosphere. *J. Atmos. Sci.*, **39**, 1972–1984.

Hoskins, B. J., 1983: Modelling of transient eddies and their feedback on the mean flow. *Large-Scale Dynamical Processes in the Atmosphere*, B. J. Hoskins and R. P. Pearce, Eds., Academic Press (in press).

Jeffreys, H., 1926: On the dynamics of geostrophic winds. *Quart. J. Roy. Meteor. Soc.*, **52**, 85–104.

Lau, N.-C., 1979: The observed structure of tropospheric stationary waves and the local balances of vorticity and heat. *J. Atmos. Sci.*, **36**, 996–1016.

——, G. H. White and R. L. Jenne, 1981: Circulation statistics for the extratropical Northern Hemisphere based on NMC analyses. NCAR Technical Note 171 + STR, 138 pp.

Lorenc, A., 1981: A global three-dimensional multivariate statistical interpolation scheme. *Mon. Wea. Rev.*, **109**, 701–721.

Lorenz, E. N., 1979: Forced and free variations of weather and climate. *J. Atmos. Sci.*, **36**, 1367–1376.

Physick, W. L., 1981: Winter depression tracks and climatological jet streams in the Southern Hemisphere during the FGGE year. *Quart. J. Roy. Meteor. Soc.*, **107**, 883–898.

Savijarvi, H., 1977: The interaction of the monthly mean flow and large-scale transient eddies in two different circulation types. Part II: Vorticity and temperature balance. *Geophysica*, **14**, 207–229.

——, 1978: The interaction of the monthly mean flow and large-scale transient eddies in two different circulation types. Part III: Potential vorticity balance. *Geophysica*, **15**, 1–16.

Simmons, A. J., and B. J. Hoskins, 1978: The life cycles of some nonlinear baroclinic waves. *J. Atmos. Sci.*, **35**, 414–432.

——, G. W. Branstator and J. M. Wallace, 1983: Barotropic wave propagation and instability, and atmospheric teleconnection patterns. *J. Atmos. Sci.*, **40**, 1363–1392.

Temperton, C., and D. L. Williamson, 1981: Normal mode initialization for a multilevel gridpoint model. I: Linear aspects. *Mon. Wea. Rev.*, **109**, 729–743.

Trenberth, K. E., 1981: Observed Southern Hemisphere eddy statistics at 500 mb: frequency and spatial dependence. *J. Atmos. Sci.*, **38**, 2585–2605.

——, 1982: Seasonality in Southern Hemisphere eddy statistics at 500 mb. *J. Atmos. Sci.*, **39**, 2507–2520.

van Loon, H., 1980: Transfer of sensible heat by transient eddies in the atmosphere on the Southern Hemisphere: An appraisal of data before and during FGGE. *Mon. Wea. Rev.*, **108**, 1774–1781.

Wallace, J. M., and D. S. Gutzler, 1981: Teleconnections in the geopotential height field during the Northern Hemisphere winter. *Mon. Wea. Rev.*, **109**, 784–812.

White, G. H., 1982: The global circulation of the atmosphere, December 1980–November 1981, based upon ECMWF analyses. Dept. of Meteor., University of Reading, 211 pp.

Williamson, D. L., and C. Temperton, 1981: Normal mode initialization for a multilevel gridpoint model. II: Nonlinear aspects. *Mon. Wea. Rev.*, **109**, 744–757.

Young, W. R., and P. B. Rhines, 1980: Rossby wave action, enstrophy and energy in forced mean flows. *Geophys. Astrophys. Fluid Dyn.*, **15**, 39–52.